

This is a repository copy of *Structure and function of Bs164  $\beta$ -mannosidase from Bacteroides salyersiae the founding member of glycoside hydrolase family GH164.*

White Rose Research Online URL for this paper:

<https://eprints.whiterose.ac.uk/155946/>

Version: Accepted Version

---

**Article:**

Armstrong, Zachary and Davies, Gideon J orcid.org/0000-0002-7343-776X (2020)  
Structure and function of Bs164  $\beta$ -mannosidase from Bacteroides salyersiae the founding member of glycoside hydrolase family GH164. The Journal of biological chemistry. pp. 4316-4326. ISSN 1083-351X

<https://doi.org/10.1074/jbc.RA119.011591>

---

**Reuse**

Items deposited in White Rose Research Online are protected by copyright, with all rights reserved unless indicated otherwise. They may be downloaded and/or printed for private study, or other acts as permitted by national copyright laws. The publisher or other rights holders may allow further reproduction and re-use of the full text version. This is indicated by the licence information on the White Rose Research Online record for the item.

**Takedown**

If you consider content in White Rose Research Online to be in breach of UK law, please notify us by emailing [eprints@whiterose.ac.uk](mailto:eprints@whiterose.ac.uk) including the URL of the record and the reason for the withdrawal request.

Structure and function of *Bs164*  $\beta$ -mannosidase from *Bacteroides salyersiae* the founding member of glycoside hydrolase family GH164.

Authors:

Zachary Armstrong<sup>1</sup>, Gideon J. Davies<sup>1\*</sup>

From the <sup>1</sup>Structural Biology Laboratory, Department of Chemistry, The University of York, York YO10 5DD, United Kingdom

Running Title: *Structure and Function of Bs164*

\* To whom correspondence should be addressed: Gideon J. Davies: Structural Biology Laboratory, Department of Chemistry, The University of York, York YO10 5DD, United Kingdom; [gideon.davies@york.ac.uk](mailto:gideon.davies@york.ac.uk); Tel. (+44) 01904 328260

**Keywords:** Mannan, Mannose, Glycoside Hydrolase, Microbiome,  $\beta$ -Mannosidase, Gut Microbe, Symbiont, GH164, Carbohydrate Active Enzyme

---

## ABSTRACT

Recent work exploring protein sequence space has revealed a new glycoside hydrolase (GH) family (GH164) of putative mannosidases. GH164 genes are present in several commensal bacteria, implicating these genes in the degradation of dietary glycans. However, little is known about the structure, mechanism of action and substrate specificity of these enzymes. Herein we report the biochemical characterization and crystal structures of the founding member of this family (*Bs164*) from the human gut symbiont *Bacteroides salyersiae*. Previous reports of this enzyme indicated that it has  $\alpha$ -mannosidase activity, however we conclusively show that it cleaves only  $\beta$ -mannose linkages. Using NMR spectroscopy, detailed enzyme kinetics of wild-type and mutant *Bs164*, and multi-angle light scattering we found that it is a trimeric retaining  $\beta$ -mannosidase, that is susceptible to several known mannosidase inhibitors. X-ray crystallography revealed the structure of *Bs164* – the first known structure of a GH164 – at 1.91 Å resolution. *Bs164* is composed of three domains: a  $(\beta/\alpha)_8$  barrel, a trimerization domain and a  $\beta$ -sandwich domain, representing a previously unobserved structural fold for  $\beta$ -mannosidases. Structures of *Bs164* at 1.80-2.55 Å resolution in complex with the inhibitors noeuromycin, mannoimidazole or DNP 2-deoxy-2-fluoromannose reveal the residues essential for specificity and catalysis including the catalytic nucleophile (Glu297) and acid/base residue (Glu160). These findings further our knowledge

of the mechanisms commensal microbes use for nutrient acquisition.

---

## Introduction

Mannose is an essential component of protein human N-glycans (1), storage polymers – mannan and glucomannan in plants (2) and mannogen in *Leishmania* (3) – and has even been observed to play a role in enzyme substrate recognition (4). Considering the roles of mannose containing polymers, it is no surprise that nature has developed a variety of enzymes to either modify the properties of these polymers or release their stored energy. The majority of enzymes that degrade mannose polymers are classified as glycoside hydrolases (GHs). The Carbohydrate Active Enzymes (CAZy) database (5) (<http://www.cazy.org>) categorizes all known GHs into > 160 families, including several with known mannosidase activity. A major focus of recent study has centred on how the enteric bacteria employ GHs to degrade variety of polysaccharides including the mannose polymers present in the human gut (6-10), resulting in a better understanding of degradation mechanisms that underpin the nutrient acquisition by commensal bacteria.

Recent work by Helbert and co-workers (11) identified a new family of mannosidases: family GH164. This was accomplished through the combination of sequence space exploration, gene synthesis and high-throughput activity assays. The founding member of GH164 – which we shall herein refer to as *Bs164* – originates from the enteric bacterium *Bacteroides salyersiae*

CL02T12C01 and was initially reported by the authors to have  $\alpha$ -mannosidase activity. This family at present contains seventeen genes, the majority of which belong to host associated strains. However, due to the preliminary nature of this discovery very little is known about the structure, action mechanism or substrate specificity of GH164 enzymes.

Here we present the detailed biochemical and structural analysis of Bs164. In contrast to initial reports, this enzyme has no  $\alpha$ -mannosidase activity; instead, Bs164 cleaves  $\beta$ -mannosidic linkages in aryl  $\beta$ -mannosidase and manno oligosaccharides. X-ray crystal structures of Bs164 reveal a homo-trimeric quaternary structure with each individual chain containing three domains. The catalytic domain of Bs164 consists of a  $(\beta/\alpha)_8$  barrel with catalytic residues on  $\beta$ -strands 4 and 7 placing this family in clan GH-A. NMR analysis revealed a retaining mechanism and site directed mutagenesis confirmed the assignment of the nucleophile and acid/base catalytic residues. Structures of inhibitor complexes show the conserved catalytic machinery involved in substrate recognition and catalysis and provide insight into the likely conformational itinerary for mannoside hydrolysis. Taken together, this work provides a thorough biochemical basis for the  $\beta$ -mannoside hydrolysis catalyzed by GH164 enzymes.

## Results and Discussion

### Operonic context of GH164s

The GH164 genes present in the CAZy database are confined to the Bacteroidetes (5), a phylum that is well known for carbohydrate utilization operons (12). In addition to the GH164 from *B. saylorsiae* four genes originate from the *Alistipes* genus, commonly found in the human gut (13), ten from the *Capnocytophaga*, typically found in the oralpharyngeal tract (14), and one each belonging to the marine bacterium *Flammeovirga* and the lichen associated *Mucilaginibacter*. Examination of the operonic context of the GH164 gives some clue to the polysaccharides which they target (Figure 1). The locus surrounding Bs164 is limited to two other genes, a hybrid two component sensor (HTCS) and an arylsulfatase like protein, however the GH164 containing operons from *Alistipes sp.* 5NYCFAH2 and *Capnocytophaga sputigena* NCTC11097, see figure 1A, are much more elaborate. Both of these operons contain a SusC and SusD-like protein – the hallmark of polysaccharide utilization loci (12) – as well as

both endo and exo-acting GH families. The presence of GH5, a family that contains endo- $\beta$ -mannanases, and GH2, a family containing both  $\beta$ -galactosidases and  $\beta$ -mannosidases, and the absence of  $\alpha$ -mannose targeting families suggests that these operons function to degrade dietary  $\beta$ -mannan, glucomannan or galactomannan rather than N-glycans. The *B. saylorsiae* genome also contains both GH5 and GH2 encoding genes suggesting that it may also target mannans, though with enzymes from separate loci.

### Bs164 is a retaining $\beta$ -mannosidase

The Bs164 protein containing an N-terminal hexahistidine tag was purified using immobilized metal affinity chromatography followed by size exclusion chromatography. The hexahistidine tag was then removed using 3C protease, and the untagged protein was further purified using an additional size exclusion chromatography step. Bs164 eluted from the size exclusion earlier than would be expected for a 74.4 kDa protein. To determine whether Bs164 exists as a multimer in solution we subjected purified Bs164 to SEC-MALS (size exclusion chromatography with multi-angle light scattering). A single peak was observed with a calculated molecular mass of 227 kDa, signifying that Bs164 forms trimers in solution.

To assess the substrate tolerance of Bs164 we assayed the purified enzyme with a variety of synthetic aryl glycosides and manno oligosaccharides (see methods for complete list). Bs164 shows no activity towards D-xylose, D- or L-arabinose, D-galactose, D-glucose, or L-fucose containing substrates. Furthermore no activity was observed towards  $\alpha$ -D-linked mannosides, contradicting the initial report of enzyme activity by Helbert *et al* (11). Bs164 did, however, have significant activity against  $\beta$ -linked aryl mannosides with a pH optimum 5.5 (Figure 2). This pH was used in assays to characterize the specificity of this enzyme towards  $\beta$ -mannoside hydrolysis (Table 1). The specificity constant for pNP  $\beta$ -man hydrolysis was approximately 6 times that seen for MU  $\beta$ -man which we attribute to pNP being a slightly better leaving group. This enzyme is also able to hydrolyse  $\beta$ -linked manno oligosaccharides and shows comparable specificity constants for the hydrolysis of mannobiose, mannotriose and mannotetraose (Table 1) indicating that it contains a +1 subsite, but that binding in the +2 position does not greatly increase hydrolysis rates. The specificity

constants for manno oligosaccharide hydrolysis were also 2-5 times lower than those seen for pNP  $\beta$ -man, which we again attribute to the better leaving group ability of pNP.

We next sought to determine whether Bs164 employs a mechanism that results in either inversion or retention of the stereochemistry at the anomeric center. We used  $^1\text{H}$  NMR spectroscopy to monitor the enzyme-catalyzed hydrolysis of paranitrophenyl  $\beta$ -D-mannopyranoside (pNP  $\beta$ -man) over the course of time (Figure 3). This revealed that the  $\beta$ -anomer of mannose is produced immediately after the enzyme is added. The free mannose then undergoes mutarotation and the ratio between  $\alpha$ - and  $\beta$ -anomers approaches equilibrium over time. This confirms that Bs164 is a retaining mechanism  $\beta$ -mannosidase and supports a mechanism that employs a nucleophile and an acid/base residue and transits through a glycosyl-enzyme intermediate.

#### **Crystal structure of Bs164 reveals a trimeric quaternary structure**

We solved the structure of Bs164 using seleno-methionine multi-wavelength anomalous dispersion data to 2.3 Å and native protein data to 1.9 Å, see Table 2 for refinement statistics. The asymmetric unit of the P1 crystal form contains six Bs164 protomers arranged into two donut shaped trimers, consistent with the trimeric form seen in solution (Figure 4A). Each trimer-donut has an outer diameter of approximately 100 Å and an internal diameter of between 30 and 35 Å. The individual Bs164 chains contain three clearly defined domains: a modified  $(\beta/\alpha)_8$  barrel (residues 22 - 389), a domain containing a seven membered mixed  $\beta$ -sheet sandwiched between  $\alpha$ -helices (390-609), and a  $\beta$ -sheet domain (610-681) (Figure 4B). This domain architecture is quite similar to that seen for family GH42 enzymes (15), but is previously unseen for  $\beta$ -mannosidases. Furthermore, analysis using the DALI server (16) indicates that the structure with highest similarity to Bs164 (RMSD = 2.4 Å, Z-score = 22.8, 100 % coverage) is indeed a GH42  $\beta$ -galactosidase from *Bacillus circulans* sp. *alkalophilus* (PDB ID: 3TTY) also with trimeric quaternary structure (17).

The  $(\beta/\alpha)_8$  fold of domain A is found in the catalytic domain of many glycoside hydrolases and is a distinctive feature of clans GH-A, D, K and R. Domain A also contains a helix containing subdomain – atypical of  $(\beta/\alpha)_8$  folds but also observed in the GH42 family (15) –

that is present between the 4<sup>th</sup>  $\beta$ -strand and the next  $\alpha$ -helix. This domain projects along the side of the domain B and interacts with domain A of a neighbouring chain (Figure 4B). We speculate that the presence of this domain helps, in part, to stabilize the trimeric structure. Domain A shows highest similarity – by means of a Dali search (16) – to the catalytic domain from the GH42  $\beta$ -galactosidase from *Rahnella* sp. (PDB: ID code 5E9A) with RMSD of 3.2 Å and complete query coverage (18). Overlay of these two structures revealed that the nucleophile (Glu314 in 5E9A) and acid/base residue (Glu157 in 5E9A) are conserved in Bs164 and the putative catalytic nucleophile and acid/base are Glu297 and Glu160 respectively. Comparison of amino acid conservation within the GH164 family also shows that this active site is completely conserved across the family (Figure 5). The positioning of the catalytic residues on strands 4 (acid/base) and 7 (nucleophile) indicate that the GH164 belongs to clan GH-A glycoside hydrolases, which contains in addition to GH42, several other families whose members are active on  $\beta$ -mannose linkages, namely: GH2, GH5, GH26 and GH113.

The active site of Bs164 is a shallow pocket that has a much more open + binding subsites than is seen in the exo-mannosidases *BtMan2A* (9) and *CmMan5A* (19). Both *BtMan2A* and *CmMan5A*, contain tryptophan residues – Trp470, for *BtMan2A* and Trp135 for *CmMan5A* – in the positive subsites, constraining the active site, and creating a more tunnel like environment, whereas Bs164 lacks an aromatic residue in a similar position. Although the positive subsites of Bs164 are more open, there are some interactions which are consistent with other mannosidases. The residue His264 in particular most resembles a positive subsite interaction residue seen in other mannosidases. His264 residue is in the same position as both Trp289 in *CmMan5A* and Trp519 in *BtMan2A*, which are thought to form a part of the +2 subsite in these proteins. The complete conservation of His264 across the GH164 family, and its positioning suggests that this residue forms part of the +2 subsite in Bs164.

In addition to the active site, domain A also contains a chloride-binding site. The chloride ion coordinates Gln45, Thr110, and two arginine residues (Arg73 and Arg75) in a penta-coordinate, distorted square pyramidal geometry, (see Figure 4D). The chloride is present is observed in all 6 chains in the crystal structure and is observed in all of the inhibitor complexes described below. This chloride is present at a site

adjacent to the active site and one of the coordinating arginines – Arg73 – and forms a direct interaction with the catalytic nucleophile. Additionally, Arg75 projects into the active site and the two  $\eta$ -nitrogens form hydrogen-bonds with the 2- and 3-hydroxyls of the sugar residue bound at the –1 subsite, as will be described below.

Domain B bears a striking resemblance to the trimerization domain of GH42 enzymes. In GH42 structures (15,18,20) there are a number of interactions between the trimerization domain and the catalytic domain which support trimeric quaternary structure. Likewise, domain B of Bs164 interacts over a surface area of 1380 Å<sup>2</sup> per protomer that includes seven residues involved in direct hydrogen bonds and two salt bridges between chains. The corresponding interface in domain A consists of the loops connecting the last two pairs of  $\beta$ -sheets and  $\alpha$ -helices. This trimerization also likely has a role in catalysis as the interaction of residues Ser342-Ala345 and Ala347 in domain A with the domain B of the neighbouring protomer appears to help position the active site residues Arg341 and Glu346 that interact directly with the substrate, as shown in the inhibitor bound structures which are described in the next section.

Unlike the first two domains, the function of the C-terminal  $\beta$ -sandwich domain is much more difficult to infer from the structure. This domain is also present in GH42 enzymes (15,18,20) however, the role of this domain within GH42s is unknown.

### Active centre structure and catalysis

To gain further insight into the mechanism and substrate recognition and confirm the assignment of the catalytic residues we produced structures of Bs164 in complex with 2,4-dinitrophenyl 2-deoxy-2-fluoro-mannoside (DNP-2FM), noeuromycin and mannoimidazole through soaks of Bs164 crystals. Mannoimidazole and noeuromycin act as competitive inhibitors of Bs164 with inhibition constants ( $K_i$ ) of  $470 \pm 60$   $\mu$ M and  $340 \pm 40$  nM respectively. The inhibition constant for noeuromycin is well in line with previous reports of  $\beta$ -mannosidase inhibition (21,22), however inhibition by mannoimidazole notably is much worse than is seen for other  $\beta$ -mannosidases such as BtMan2A ( $K_i = 1.4$   $\mu$ M) (21). The fluorosugar DNP-2FM is a mechanism based inhibitor which forms a glycosyl-enzyme intermediate that is turned over at much slower rates than the natural sugar, thereby enabling the

identification of the catalytic nucleophile (23). All three of these inhibitors are present in the Bs164 active site –1 subsite (Figure 6).

The mannosidase inhibitors are recognized in the –1 subsite by eight polar amino acids, which are within hydrogen bonding distance to the substrate (Figure 6). All eight of these polar contacts are completely conserved across all GH164s currently within the CAZy database, and form similar interactions with each of the inhibitors. The O6 sits, pointing towards the  $\beta$ -face between the carbonyl of Glu346 and the indole nitrogen of Trp263. Glu346 is also positioned to hydrogen bond O4 of the inhibitors, the Glu-O4-O6 motif is seen in a number of mannosidase structures including those for GH1 (PDB ID: 4RE2) (24), GH2 (PDB ID: 2VMF) (21), and GH5 (PDB ID: 1UZ4) (22). The O4 of all inhibitors hydrogen bonds with Arg341, is part of a loop that interacts with the trimerization domain of the neighbouring protomer. Another arginine, Arg75 (which is bound to chlorine) hydrogen bonds to O3 of all inhibitors and the O2 of mannoimidazole and noeuromycin. Arg75 lies below the sugar plane and likely provides impetus for the O2 axial to equatorial migration, the presence of an arginine bridging the O2 and O3 hydroxyls is also seen in the GH113  $\beta$ -mannanase AaManA (25). The O2 hydroxyl also hydrogen bonds to Asn159 in all three inhibitor structures and the nucleophile (Glu297) in mannoimidazole and noeuromycin structures. The hydrophobic element on the  $\alpha$ -face of the sugar is provided by Trp336, well within range to form CH- $\pi$  interactions – a motif which is often seen in protein- $\beta$ -mannose interactions (26).

The structure of bound 2FM clearly shows a covalent intermediate attached to Glu297, this observation along with kinetic analysis of an E297Q variant conclusively identifies Glu297 as the active site nucleophile. The acid/base residue, Glu160 is positioned to perform *anti*-protonation of the leaving group, typical of clan GH-A glycoside hydrolases (27). This residue forms hydrogen bonding interactions with both the endocyclic nitrogen in noeuromycin and imidazole nitrogen in mannoimidazole, an interaction which is also seen in GH26 and GH113  $\beta$ -mannanases (25) and GH2  $\beta$ -mannosidases (21). Further evidence, in the form of near complete loss of activity by the E160Q variant (see Table 1) confirms the assignment of Glu160 as the acid/base residue.

The inhibitor bound structures of Bs164 also give insight into the conformational itinerary

of  $\beta$ -mannoside hydrolysis. Most  $\beta$ -mannosidases and  $\beta$ -mannanases, including families GH2, GH5, GH26, GH113 and GH130 have been observed to transit through a  ${}^1S_5 \rightarrow B_{2,5}^\ddagger \rightarrow {}^0S_2$  glycosylation itinerary (28), the outlier being the inverting enzyme GH134 which instead proceeds through  ${}^1C_4 \rightarrow {}^3H_4^\ddagger \rightarrow {}^3S_1$  (see reference (29)). The structure of the mannoimidazole – an inhibitor which faithfully reports on the transition state of mannosidases (21,25,28,30) – is clearly in a  $B_{2,5}$  conformation within the *Bs164* active site (figure 6, B) indicating that the conformational itinerary is centred, as for most  $\beta$ -mannosidases, around a  $B_{2,5}$  transition state. The structure of the noeuromycin complex, in which a  ${}^1S_5$  conformation is observed (figure 6A), lends further support to this itinerary. Observations from other  $\beta$ -mannosidases (28,31) suggest we should expect the glycosyl-enzyme intermediate to adopt a  ${}^0S_2$  conformation, however, in the complex with 2FM the ring is in a  ${}^4C_1/E_5$  conformation ( $\varphi = 295^\circ$ ,  $\theta = 37^\circ$ ) with the 2F positioned axially, instead of equatorially as would be expected in a  ${}^0S_2$  conformation. The comparatively low resolution of the 2FM structure (2.55 Å) makes it difficult to equivocally confirm the conformation of the glycosyl-enzyme intermediate that appears to refine as  ${}^4C_1/E_5$ . We endeavour to further explore the energetic consequences of this  ${}^4C_1/E_5$  conformation and whether this is the structure is representative of the true glycosyl-enzyme intermediate or an energetic relaxation of this intermediate to a position that is not along the conformational itinerary.

## Conclusions

The capacity of commensal bacterial to digest dietary carbohydrates relies on a broad range of enzymes, tailored to their specific target. Examination of *Bs164*, the prototypical GH164, adds to our growing understanding of the mechanisms underpinning enteric carbohydrate degradation. Our interrogation of this enzyme has shown that it exists as a donut shaped homotrimer – a new domain architecture and quaternary structure for  $\beta$ -mannosidases – and employs two conserved glutamic acid residues in a retaining mechanism. The structural analysis of *Bs164* in the presence of inhibitors revealed a host of active site interactions and suggested a boat-like transition state. Further investigation of how the genes co-localized within GH164 containing operons, promises to reveal how these loci function in concert to enable degradation of

mannose containing polymers within the human microbiome.

## Experimental procedures

### Substrates and Inhibitors

Paranitrophenyl  $\beta$ -D-mannopyranoside and methylumbelliferyl  $\beta$ -D-mannopyranoside were purchased from Sigma-Aldrich. Mannobiose, mannotriose and mannotetraose were purchased from Megazyme (Bray, Ireland). Mannoimidazole and noeuromycin were kind gifts from Professor Spencer Williams and Professor Robert V. Stick, respectively. 2,4-dinitrophenyl 2-deoxy-2-fluoro- $\beta$ -D-mannopyranoside was a kind gift from Professor Stephen G Withers (University of British Columbia).

### Gene expression and protein purification

The gene encoding *Bs164* (GenBank accession EIY59668.1) was predicted to contain a signal peptide with a cleavage site between amino acids 21 and 22 by signalP 5.0 (32). A codon optimized version of this gene with a hexahistidine tag in place of the signal peptide (MGSSHHHHHSSGLEVLFGPA) was synthesized by and cloned into a pET-28 vector by Genscript (Leiden, Netherlands). Plasmid was transformed into chemically competent BL21 (*DE3*) gold cells (Agilent) and plated on LB agar containing 50  $\mu$ g/mL kanamycin. A single colony was used to inoculate a 5 mL of LB media containing 50  $\mu$ g/mL kanamycin. After overnight growth at 37 °C with shaking at 180 rpm this starter culture was used to inoculate NZYTech auto-induction media (NZYTech) containing 50  $\mu$ g/mL kanamycin. Expression cultures were grown at 37 °C with shaking at 250 rpm for 6 h, the temperature was then decreased to 20 °C and cultures were incubated for an additional 22 h. Expression cultures were harvested by centrifugation (5,000 x g, 30 min, 4 °C) and cell pellets were stored at -80 °C until purification.

To purify the protein cell pellets were resuspended in 120 mL of Buffer A (50 mM HEPES, 30 mM imidazole, 200 mM NaCl, pH 7.4) with additional protease inhibitor (4-[2-aminoethyl]benzenesulfonyl fluoride, 0.1 mM) lysozyme, and DNase. Resuspended cells were then lysed by passage through a cell-disruptor homogenizer at 25 kpsi. Lysed cells were centrifuged (18,000 x g, 30 min, 4 °C) and the supernatant was decanted from the cell debris. Clarified supernatant was loaded directly onto a 5 mL Histag Excel column (GEHealthcare). Bound

protein was washed with 7.5 column volumes of buffer A then eluted with a linear gradient of 0-100 % buffer B (50 mM HEPES pH 7.4, 1 M imidazole, 200 mM NaCl) over 20 column volumes. Eluted protein was concentrated with a 30 kDa cut-off Amicon centrifugal filter unit and further purified by gel filtration (HiLoad 16/600 Superdex 200 pg; GE Healthcare) in buffer C (50 mM HEPES, 200 mM NaCl, pH 7.4). The purity of eluted protein was analysed by SDS-PAGE and the peak fractions were pooled and concentrated with a 30 kDa cutoff Amicon centrifugal filter unit. Concentrated protein was washed with buffer D (20 mM HEPES, pH 7.4) then diluted to 30 mg/mL with buffer D and flash frozen with liquid nitrogen until use. Protein concentrations were determined spectrophotometrically using a calculated  $A_{280}$  extinction coefficient of  $128,480 \text{ M}^{-1}\text{cm}^{-1}$ . For biochemical studies, the N-terminal hexa-histidine tag was cleaved from Bs164 through overnight incubation with a 1:100 ratio (by mass) of 3C-protease. Cleaved Bs164 was then purified by gel filtration and concentrated as detailed above. The average yield of purified protein was approximately 30 mg per litre of culture.

Seleno-methionine labelled protein was expressed using the same bacterial strain as for the wild-type protein. This strain was used to inoculate 40 mL LB media containing 50  $\mu\text{g/mL}$  kanamycin which was grown overnight at 37 °C. This culture was then centrifuged (3,000 x g, 10 min, 4 °C) and the cell pellet was resuspended in 40 mL of M9 media containing 50  $\mu\text{g/mL}$  kanamycin. The resuspended cells (1 mL) were then used to inoculate a 1 L culture of M9 media containing 50  $\mu\text{g/mL}$  kanamycin. This culture was incubated at 37 °C with shaking at 250 rpm until mid-log phase ( $\text{OD}_{600} = 0.5$ ). At this point lysine (100 mg/L), phenylalanine (100 mg/L), threonine (100 mg/L), isoleucine (50 mg/L), leucine (50 mg/L), valine (50 mg/L) and seleno-methionine (50 mg/L) were added to the culture, which was incubated for another 15 min at 37 °C. The incubation temperature was then lowered to 20 °C and IPTG was added to a final concentration of 0.5 mM. After incubation for 18 h the cultures were harvested as for the unlabelled protein. The seleno-methionine protein was purified as for the unlabelled protein except for the addition of 5 mM DTT to buffers A, B and C and the addition of 0.5 mM TCEP to buffer D.

Mutagenesis was performed using a modified Quikchange™ (Agilent) protocol. For each mutant generated, PCR was first performed

for 12 cycles with one of the sense or antisense primers (E288Q\_F: GTG GCT GAT GAC CCA ACT GCA AGG TG, E288Q\_R: CAC CTT GCA GTT GGG TCA TCA GCC AC, E151Q\_F: GTG CTG ATT AAC CAG CCG GGT ACC C, E151Q\_R: GGG TAC CCG GCT GGT TAA TCA GCA C); these two reactions were subsequently pooled, and an additional 18 cycles of PCR were performed. PCR products were digested with DpnI (NEB) and transformed into chemically competent BL21 (DE3) gold cells. Purified plasmids were sequenced to confirm the correct mutation prior to expression. Both the nucleophile and acid base variants were purified as for the wild-type protein.

### Activity assays

All Bs164 activity assays, unless otherwise stated, were performed at 25 °C in a buffer containing 80 mM MES pH 5.5 and 160 mM NaCl, and were initiated by the addition of the appropriate amount of enzyme. Purified Bs164 was initially tested for activity on the following aryl glycosides: pNP  $\alpha$ -L-arabinofuranoside, pNP  $\alpha$ -L-arabinopyranoside, pNP  $\alpha$ -L-fucopyranoside, pNP  $\beta$ -D-galactopyranoside, pNP  $\alpha$ -D-glucopyranoside, pNP  $\beta$ -D-glucopyranoside, pNP  $\alpha$ -D-mannopyranoside, pNP  $\beta$ -D-mannopyranoside, and pNP  $\beta$ -D-xylopyranoside. Purified enzyme was added (final concentration of 1  $\mu\text{M}$ ) to a solution of 1 mM substrate. These assays were incubated at 25 °C and were stopped after 6 h with a 1:1 ratio of 1M  $\text{Na}_2\text{CO}_3$  (pH 11.2) and absorbance at 400 nm was measured with a CLARIOstar Plus plate reader (BMG Labtech).

The optimal pH for activity was determined with methylumbelliferyl  $\beta$ -D-mannopyranoside (MU  $\beta$ -man) using substrate depletion kinetics. Purified enzyme was added to solutions containing 50  $\mu\text{M}$  MU  $\beta$ -man, 160 mM NaCl and either MES (pH 5-6.5) or HEPES (pH 6.5-8.5). Reactions were limited to this pH range as enzyme denaturation was observed above pH 8.5 and below pH 5. Fluorescence was monitored continuously ( $\lambda_{\text{ex}} = 365 \text{ nm}$ ,  $\lambda_{\text{em}} = 450 \text{ nm}$ ) and depletion curves were fit to the equation  $A = A_0(1 - e^{-kt})$ , where  $k = [\text{E}] \cdot k_{\text{cat}}/K_M$ , to give the specificity constant at each pH.

Kinetic parameters were determined for pNP  $\beta$ -Man and MU  $\beta$ -Man using substrate concentrations covering the range of 1/5 to 5 times the eventual  $K_M$  determined. Assays were performed in 96 well plates and each plate included either pNP or MU standards in an identical buffer system for concentration

calibration. MU  $\beta$ -man hydrolysis was monitored continuously ( $\lambda_{\text{ex}} = 365 \text{ nm}$  and  $\lambda_{\text{em}} = 450 \text{ nm}$ ) while pNP  $\beta$ -man hydrolysis was measured after stopping the assay with a 1:1 ratio of 1M  $\text{Na}_2\text{CO}_3$  (pH 11.2).

The specificity constant for the hydrolysis of mannobiose, mannotriose and mannotetraose was determined using an assay for reducing sugars employing bicinchoninic acid (BCA). Reactions containing between 0.1 and 4 mM mannobiose were incubated at 25 °C and aliquots were removed over a period of 30 min. These aliquots were added to an equal volume of freshly prepared BCA reagent containing: 400 mM sodium carbonate pH 11.2, 2.5 mM Bicinchoninic acid, 1.25 mM  $\text{CuSO}_4$  and 2.5 mM L-serine. This mixture was heated to 80 °C for 10 min, and then cooled. The absorbance at 563 nm was measured with a CLARIOstar Plus plate reader (BMG Labtech) and compared to a standard curve of mannose to calculate the concentration of reducing sugars. Data was fit to linear equation to give the specificity constant.

To determine inhibition constant ( $K_i$ ) values Michaelis-Menten parameters were determined for Bs164 hydrolysis of pNP  $\beta$ -man in reactions containing either mannoimidazole or noeuromycin. Assays were started with the addition of enzyme to the assay mix. Parameters were determined for at least 3 different inhibitor concentrations. Inhibition constants were calculated according to a competitive inhibition model for both inhibitors. All kinetic parameters were fit with the software program Origin 2019.

### SEC-MALS

Experiments were conducted on a system comprising a Wyatt HELEOS-II multi-angle light scattering detector and a Wyatt rEX refractive index detector linked to a Shimadzu HPLC system (SPD-20A UV detector, LC20-AD isocratic pump system, DGU-20A3 degasser and SIL-20A autosampler). Work was conducted at room temperature ( $20 \pm 2 \text{ }^\circ\text{C}$ ). Sample injection volume was 100  $\mu\text{L}$  at a protein concentration of 5 mg/ml. The samples were separated on a Superdex S200 10/300 (GE Healthcare) using 80 mM MES pH 5.5, 200 mM NaCl as buffer. Shimadzu LC Solutions software was used to control the HPLC and Astra V software for the HELEOS-II and rEX detectors. Data were analysed using the Astra V software. MWs were estimated using the Zimm fit method (33) with degree 1. A value of 0.19 was used for protein refractive index increment ( $\text{dn}/\text{dc}$ ).

### NMR

Prior to NMR experiments buffer (80 mM MES pH 5.5 and 160 mM NaCl), pNP  $\beta$ -mannoside and Bs164 were lyophilized. Buffer and enzyme were resuspended in  $\text{D}_2\text{O}$ , while pNP  $\beta$ -mannoside was resuspended in 10 %  $\text{d}_6$ -DMSO in  $\text{D}_2\text{O}$ . The final reaction mixture contained 4.5 mM pNP  $\beta$ -man, 9 mM MES (pH 5.5), 145 mM NaCl, and 0.9 % (v/v)  $\text{d}_6$ -DMSO. NMR spectra were collected before the addition of enzyme and every 5 min after the addition of Bs164 to a final concentration of 120  $\mu\text{g}/\text{mL}$ . NMR data was collected on a Bruker 700 MHz Avance Neo spectrometer equipped with a 5 mm triple resonance cryoprobe. 1-D proton spectra were recorded with a 30 degree excitation pulse, an interscan delay of 10 s and a total acquisition time of 3 min. Sample temperature was maintained at 298 K, and referencing was relative to DSS.

### Crystallization and structure determination

His<sub>6</sub>-Bs164 at 30 mg/mL was tested against a range of commercial crystallization screens. Large split crystals were found in 100 mM ammonium tartrate dibasic pH 7.0, 12% w/v PEG 3,350, a condition that was used for further optimization. Crystals formed in 0.1 M ammonium tartrate dibasic at a pH range from 5.5 to pH 7.0. The optimized crystals were grown in maxi 48-well plates using the sitting-drop vapor-diffusion method at 20 °C with 100 mM Ammonium tartrate dibasic pH 7.0, 13% w/v PEG 3,350 with a protein: well solution ration of 500:500 nL. Crystals were soaked in well solution containing 25% (v/v) ethylene glycol before flash cooling in liquid nitrogen. Inhibitor complexes were obtained by soaking crystals in well solution containing 10 mM of the inhibitor for 3–4 h before flash cooling in liquid nitrogen. For the structures with DNP 2FM solid substrate was added to the drop containing crystals and which were then soaked overnight. The overnight soaking with crystals of DNP 2FM gave inhibitor complexes, but did appear to reduce diffraction quality. Refinement statistics are given in Table 2.

Bs164 seleno-methionine derivative, mannoimidazole, noeuromycin, DNP 2FM diffraction data were collected at Diamond beamlines, and data were processed with the CCP4i2 suite (34). The unliganded structure of Bs164 was solved by MAD phasing of a seleno-methionine derivative using 6 datasets: two at the peak wavelength (0.9794Å) using 0.1° oscillation and a  $\chi$  angle of 25° or 0°, for 360°; two at a



remote wavelength (0.9777 Å) using 0.1° oscillation and a  $\chi$  angle of 25° or 0°, for 360° and two at the inflection (0.9797 Å) using 0.1° oscillation and a  $\chi$  angle of 25° or 0°, for 360°. Crank2 (35) was used for phasing and initial model building. Cycles of maximum-likelihood refinement using REFMAC5 (36) were interspersed with manual corrections of the models using COOT (37). Complexed structures of Bs164 were solved by molecular replacement using the unliganded coordinates as the search model in Phaser (38). Structural figures were drawn with PyMol (DeLano Scientific LLC, <http://pymol.sourceforge.net/>).

### Sequence Alignment

All Seventeen GH164 sequences currently available in the CAZy database (5) (Accessed 01-12-2019) were aligned using the COBALT multiple sequence alignment tool (39) and amino acid conservation was determined using the ConSurf server (40) and visualized in PyMol.

### Data availability

The atomic coordinates and structure factors have been deposited in the Protein Data Bank. PDB ID codes: 6T5O, 6T75, 6T6G, 6T7G.

### ACKNOWLEDGEMENTS

We would like to thank Andrew Leech, University of York Bioscience Technology Facility, for assistance with SEC-MALS and Alex Heyam, University of York NMR Facility, for assistance with <sup>1</sup>H NMR experiments. We also thank Professor Spencer J. Williams, Professor Stephen G. Withers, and Professor Robert V. Stick for providing us with enzyme inhibitors. We thank Diamond Light Source for access to beamline i04 (proposal number mx-18598-38) that contributed to the results presented here and Johan Turkenburg and Sam Hart for coordinating data collection. We also thank Biotechnology and Biological Sciences Research Council (BBSRC; BB/R001162/1 and BB/M011151/1 grants to G.J.D.). GJD thanks the Royal Society for the Ken Murray Research Professorship.

### Conflict of Interest

The authors declare that they have no conflicts of interest with the contents of this article.

### References

1. Lowe, J. B., and Marth, J. D. (2003) A genetic approach to mammalian glycan function. *Annual Review of Biochemistry* **72**, 643-691
2. Yu, L., Lyczakowski, J. J., Pereira, C. S., Kotake, T., Yu, X., Li, A., Mogelsvang, S., Skaf, M. S., and Dupree, P. (2018) The patterned structure of galactoglucomannan suggests it may bind to cellulose in seed mucilage. *Plant Physiology* **178**, 1011-1026
3. Sernee, M. F., Ralton, J. E., Nero, T. L., Sobala, L. F., Kloehn, J., Vieira-Lara, M. A., Cobbold, S. A., Stanton, L., Pires, D. E. V., Hanssen, E., Males, A., Ward, T., Bastidas, L. M., van der Peet, P. L., Parker, M. W., Ascher, D. B., Williams, S. J., Davies, G. J., and McConville, M. J. (2019) A family of dual-activity glycosyltransferase-phosphorylases mediates mannogen turnover and virulence in *Leishmania* parasites. *Cell Host & Microbe* **26**, 385-399.e389
4. Bie, H., Yin, J., He, X., Kermode, A. R., Goddard-Borger, E. D., Withers, S. G., and James, M. N. G. (2013) Insights into mucopolysaccharidosis I from the structure and action of  $\alpha$ -L-iduronidase. *Nature Chemical Biology* **9**, 739-745
5. Lombard, V., Golaconda Ramulu, H., Drula, E., Coutinho, P. M., and Henrissat, B. (2014) The carbohydrate-active enzymes database (CAZy) in 2013. *Nucleic Acids Research* **42**, D490-495
6. Gregg, K. J., Zandberg, W. F., Hehemann, J.-H., Whitworth, G. E., Deng, L., Vocadlo, D. J., and Boraston, A. B. (2011) Analysis of a new family of widely distributed metal-independent  $\alpha$ -mannosidases provides unique insight into the processing of N-linked glycans. *Journal of Biological Chemistry* **286**, 15586-15596
7. Zhu, Y., Suits, M. D. L., Thompson, A. J., Chavan, S., Dinev, Z., Dumon, C., Smith, N., Moremen, K. W., Xiang, Y., Siriwardena, A., Williams, S. J., Gilbert, H. J., and Davies, G. J. (2009) Mechanistic insights into a Ca<sup>2+</sup>-dependent family of  $\alpha$ -mannosidases in a human gut symbiont. *Nature Chemical Biology* **6**, 125-132
8. Cuskin, F., Lowe, E. C., Temple, M. J., Zhu, Y., Cameron, E. A., Pudlo, N. A., Porter, N. T., Urs, K., Thompson, A. J., Cartmell, A., Rogowski, A., Hamilton, B. S., Chen, R., Tolbert, T. J., Piens, K., Bracke, D., Verweken, W., Hakki, Z., Speciale, G., Munõz-Munõz, J. L., Day, A., Peña, M. J., McLean, R., Suits, M. D., Boraston, A. B., Atherly, T., Ziemer, C. J., Williams, S. J., Davies, G. J., Abbott, D. W., Martens, E. C., and Gilbert, H. J. (2015) Human gut Bacteroidetes can utilize yeast mannan through a selfish mechanism. *Nature* **517**, 165-169
9. Tailford, L. E., Money, V. A., Smith, N. L., Dumon, C., Davies, G. J., and Gilbert, H. J. (2007) Mannose foraging by *Bacteroides thetaiotaomicron*. *Journal of Biological Chemistry* **282**, 11291-11299
10. Bågenholm, V., Reddy, S. K., Bouraoui, H., Morrill, J., Kulcinskaja, E., Bahr, C. M., Aurelius, O., Rogers, T., Xiao, Y., Logan, D. T., Martens, E. C., Koropatkin, N. M., and Ståhlbrand,

- H. (2017) Galactomannan catabolism conferred by a polysaccharide utilization locus of *Bacteroides ovatus*. *Journal of Biological Chemistry* **292**, 229-243
11. Helbert, W., Poulet, L., Drouillard, S., Mathieu, S., Loidice, M., Couturier, M., Lombard, V., Terrapon, N., Turchetto, J., Vincentelli, R., and Henrissat, B. (2019) Discovery of novel carbohydrate-active enzymes through the rational exploration of the protein sequences space. *Proceedings of the National Academy of Sciences* **116**, 6063-6068
  12. Lapébie, P., Lombard, V., Drula, E., Terrapon, N., and Henrissat, B. (2019) Bacteroidetes use thousands of enzyme combinations to break down glycans. *Nature Communications* **10**
  13. Gilbert, J. A., Martínez, I., Muller, C. E., and Walter, J. (2013) Long-term temporal analysis of the human fecal microbiota revealed a stable core of dominant bacterial species. *PLoS ONE* **8**, e69621
  14. Jolivet-Gougeon, A., Sixou, J.-L., Tamanai-Shacoori, Z., and Bonnaure-Mallet, M. (2007) Antimicrobial treatment of *Capnocytophaga* infections. *International Journal of Antimicrobial Agents* **29**, 367-373
  15. Hidaka, M., Fushinobu, S., Ohtsu, N., Motoshima, H., Matsuzawa, H., Shoun, H., and Wakagi, T. (2002) Trimeric crystal structure of the glycoside hydrolase family 42 beta-galactosidase from *Thermus thermophilus* A4 and the structure of its complex with galactose. *Journal of molecular biology* **322**, 79-91
  16. Holm, L. (2019) Benchmarking fold detection by DaliLite v.5. *Bioinformatics*
  17. Maksimainen, M., Paavilainen, S., Hakulinen, N., and Rouvinen, J. (2012) Structural analysis, enzymatic characterization, and catalytic mechanisms of  $\beta$ -galactosidase from *Bacillus circulans* sp. *alkalophilus*. *FEBS Journal* **279**, 1788-1798
  18. Fan, Y., Hua, X., Zhang, Y., Feng, Y., Shen, Q., Dong, J., Zhao, W., Zhang, W., Jin, Z., and Yang, R. (2015) Cloning, expression and structural stability of a cold-adapted  $\beta$ -galactosidase from *Rahnella* sp. R3. *Protein Expression and Purification* **115**, 158-164
  19. Dias, F. M. V., Vincent, F., Pell, G., Prates, J. A. M., Centeno, M. S. J., Tailford, L. E., Ferreira, L. M. A., Fontes, C. M. G. A., Davies, G. J., and Gilbert, H. J. (2004) Insights into the molecular determinants of substrate specificity in glycoside hydrolase family 5 revealed by the crystal structure and kinetics of *Cellvibrio mixtus* mannosidase 5A. *Journal of Biological Chemistry* **279**, 25517-25526
  20. Viborg, A. H., Katayama, T., Arakawa, T., Abou Hachem, M., Lo Leggio, L., Kitaoka, M., Svensson, B., and Fushinobu, S. (2017) Discovery of  $\alpha$ -L-arabinopyranosidases from human gut microbiome expands the diversity within glycoside hydrolase family 42. *Journal of Biological Chemistry* **292**, 21092-21101
  21. Tailford, L. E., Offen, W. A., Smith, N. L., Dumon, C., Morland, C., Gratien, J., Heck, M.-P., Stick, R. V., Blériot, Y., Vasella, A., Gilbert, H. J., and Davies, G. J. (2008) Structural and biochemical evidence for a boat-like transition state in  $\beta$ -mannosidases. *Nature Chemical Biology* **4**, 306-312
  22. Vincent, F., Gloster, T. M., Macdonald, J., Morland, C., Stick, R. V., Dias, F. M. V., Prates, J. A. M., Fontes, C. M. G. A., Gilbert, H. J., and Davies, G. J. (2004) Common inhibition of both  $\beta$ -glucosidases and  $\beta$ -mannosidases by isofagomine lactam reflects different conformational itineraries for pyranoside hydrolysis. *ChemBioChem* **5**, 1596-1599
  23. Stoll, D., He, S., Withers, S. G., and Warren, R. A. (2000) Identification of Glu-519 as the catalytic nucleophile in beta-mannosidase 2A from *Cellulomonas fimi*. *The Biochemical journal* **351 Pt 3**, 833-838
  24. Tankrathok, A., Iglesias-Fernández, J., Williams, R. J., Pengthaisong, S., Baiya, S., Hakki, Z., Robinson, R. C., Hrmova, M., Rovira, C., Williams, S. J., and Ketudat Cairns, J. R. (2015) A single glycosidase harnesses different pyranoside ring transition state conformations for hydrolysis of mannosides and glucosides. *ACS Catalysis* **5**, 6041-6051
  25. Williams, R. J., Iglesias-Fernández, J., Stepper, J., Jackson, A., Thompson, A. J., Lowe, E. C., White, J. M., Gilbert, H. J., Rovira, C., Davies, G. J., and Williams, S. J. (2014) Combined inhibitor free-energy landscape and structural analysis reports on the mannosidase conformational coordinate. *Angewandte Chemie International Edition* **53**, 1087-1091
  26. Hudson, K. L., Bartlett, G. J., Diehl, R. C., Agirre, J., Gallagher, T., Kiessling, L. L., and Woolfson, D. N. (2015) Carbohydrate-aromatic interactions in proteins. *Journal of the American Chemical Society* **137**, 15152-15160
  27. Nerinckx, W., Desmet, T., Piens, K., and Claeysens, M. (2005) An elaboration on the *syn-antiproton* donor concept of glycoside hydrolases: electrostatic stabilisation of the transition state as a general strategy. *FEBS Letters* **579**, 302-312
  28. Rovira, C., Males, A., Davies, G. J., and Williams, S. J. (2019) Mannosidase mechanism: At the intersection of conformation and catalysis. *Current Opinion in Chemical Biology* **53**, Accepted, in press
  29. Jin, Y., Petricevic, M., John, A., Raich, L., Jenkins, H., Portela De Souza, L., Cuskin, F., Gilbert, H. J., Rovira, C., Goddard-Borger, E. D., Williams, S. J., and Davies, G. J. (2016) A  $\beta$ -mannanase with a lysozyme-like fold and a novel molecular catalytic mechanism. *ACS Central Science* **2**, 896-903
  30. Males, A., Speciale, G., Williams, S. J., and Davies, G. J. (2019) Distortion of mannoimidazole supports a B<sub>2,5</sub> boat transition state for the family GH125  $\alpha$ -1,6-mannosidase from *Clostridium perfringens*. *Organic & Biomolecular Chemistry* **17**, 7863-7869
  31. Ducros, V. M., Zechel, D. L., Murshudov, G. N., Gilbert, H. J., Szabo, L., Stoll, D., Withers, S. G., and Davies, G. J. (2002) Substrate distortion by a beta-mannanase: snapshots of the Michaelis and covalent-intermediate complexes suggest a B<sub>2,5</sub>

- conformation for the transition state. *Angewandte Chemie* **41**, 2824-2827
32. Almagro Armenteros, J. J., Tsirigos, K. D., Sønderby, C. K., Petersen, T. N., Winther, O., Brunak, S., von Heijne, G., and Nielsen, H. (2019) SignalP 5.0 improves signal peptide predictions using deep neural networks. *Nature Biotechnology* **37**, 420-423
33. Zimm, B. H. (1945) Molecular theory of the scattering of light in fluids. *The Journal of Chemical Physics* **13**, 141-145
34. Potterton, L., Agirre, J., Ballard, C., Cowtan, K., Dodson, E., Evans, P. R., Jenkins, H. T., Keegan, R., Krissinel, E., Stevenson, K., Lebedev, A., McNicholas, S. J., Nicholls, R. A., Noble, M., Pannu, N. S., Roth, C., Sheldrick, G., Skubak, P., Turkenburg, J., Uski, V., von Delft, F., Waterman, D., Wilson, K., Winn, M., and Wojdyr, M. (2018) CCP4i2: the new graphical user interface to the CCP4 program suite. *Acta Crystallographica Section D Structural Biology* **74**, 68-84
35. Skubák, P., and Pannu, N. S. (2013) Automatic protein structure solution from weak X-ray data. *Nature Communications* **4**
36. Murshudov, G. N., Skubák, P., Lebedev, A. A., Pannu, N. S., Steiner, R. A., Nicholls, R. A., Winn, M. D., Long, F., and Vagin, A. A. (2011) REFMAC5 for the refinement of macromolecular crystal structures. *Acta Crystallographica Section D Biological Crystallography* **67**, 355-367
37. Emsley, P., Lohkamp, B., Scott, W. G., and Cowtan, K. (2010) Features and development of COOT. *Acta Crystallographica Section D Biological Crystallography* **66**, 486-501
38. McCoy, A. J., Grosse-Kunstleve, R. W., Adams, P. D., Winn, M. D., Storoni, L. C., and Read, R. J. (2007) Phaser crystallographic software. *Journal of Applied Crystallography* **40**, 658-674
39. Papadopoulos, J. S., and Agarwala, R. (2007) COBALT: constraint-based alignment tool for multiple protein sequences. *Bioinformatics* **23**, 1073-1079
40. Ashkenazy, H., Abadi, S., Martz, E., Chay, O., Mayrose, I., Pupko, T., and Ben-Tal, N. (2016) ConSurf 2016: an improved methodology to estimate and visualize evolutionary conservation in macromolecules. *Nucleic Acids Research* **44**, W344-W350
41. Moreira, L. R. S., and Filho, E. X. F. (2008) An overview of mannan structure and mannan-degrading enzyme systems. *Applied Microbiology and Biotechnology* **79**, 165-178

#### Abbreviations

CAZy: Carbohydrate Active enzyme database; DNP-2FM: 2,4-dinitrophenyl 2-deoxy-2-fluoro- $\beta$ -D-mannopyranoside; HCTS: Hybrid Two-Component System; Hyp: Hypothetical; MU: 4-methylumbelliferyl; MU  $\beta$ -man: 4-methylumbelliferyl  $\beta$ -D-mannopyranoside; PDB: Protein Data Bank; pNP: paranitrophenyl; pNP  $\beta$ -man: paranitrophenyl  $\beta$ -D-mannopyranoside; RMSD: root-mean-square deviation

Table 1. Kinetic parameters of mannoside hydrolysis for Bs164 and mutants.

Enzyme	Substrate	$k_{\text{cat}}$ ( $\text{s}^{-1}$ )	$K_{\text{M}}$ (mM)	$k_{\text{cat}} / K_{\text{M}}$ ( $\text{s}^{-1} \cdot \text{mM}^{-1}$ )
Bs164	pNP $\beta$ -man	$40 \pm 3$	$3.6 \pm 0.8$	$11 \pm 3$
Bs164	MU $\beta$ -man	$1.8 \pm 0.05$	$1.05 \pm 0.08$	$1.7 \pm 0.1$
Bs164	Mannobiose	-	-	$2.2 \pm 0.4$
Bs164	Mannotriose	-	-	$5.6 \pm 0.7$
Bs164	Mannotetraose	-	-	$4.5 \pm 0.7$
Bs164_E297Q	pNP $\beta$ -man	$0.124 \pm 0.003$	$0.87 \pm 0.05$	$0.14 \pm 0.01$
Bs164_E160Q	pNP $\beta$ -man	-	-	$< 10^{-6}$ *

\* Estimated from limit of detection

Table 2. Data collection and refinement statistics

	SeMet-Bs164			"Apo"-Bs164 (6T5O)	2-F-Mannose (6T75)	Mannoimidazole (6T7G)	Noeruomycin (6T6G)
<b>Data collection</b>							
Space group	P1			P1	P1	P1	P1
<b>Cell dimensions</b>							
<i>a, b, c</i> (Å)	69.5, 104.5, 170.4			69.2, 103.9, 169.2	70.2, 104.9, 171.6	69.7, 104.7, 170.6	69.8, 105.1, 170.5
$\alpha, \beta, \gamma$ (°)	92.3, 97.4, 106.2,			92.5 97.3, 106.4	92.0, 97.7, 107.2	92.3, 97.3, 106.3	92.6, 97.2, 105.1
	Peak	Inflection	Remote				
Wavelength (Å)	0.9794	0.9797	0.9777	0.9795	0.9763	0.97623	0.9159
Resolution (Å)	67.13-2.30 (2.34-2.30)	67.13-2.30 (2.34-2.30)	67.13-2.30 (2.34-2.30)	66.76- 1.91(1.94- 1.91)	99.90-2.54 (2.59- 2.55)	168.66-1.79 (1.83-1.80)	101.13-2.06 (2.10-2.06)
<i>R</i> <sub>merge</sub>	0.070 (0.297)	0.074 (0.338)	0.086 (0.477)	0.062 (0.546)	0.113 (1.073)	0.044 (0.548)	0.115 (1.039)
<i>I</i> / $\sigma I$	15.3 (4.9)	15.3 (4.7)	14.5 (4.0)	9.4 (1.6)	6.1 (1.0)	6.5 (1.1)	5.2 (1.0)
Completeness (%)	99.9 (97.9)	99.9 (97.9)	99.9 (97.9)	95.6 (93.1)	98.7 (98.0)	100.0 (100.0)	98.3 (97.4)
Redundancy	7.0 (7.0)	7.0 (7.0)	7.0 (7.0)	3.2 (3.2)	3.6 (3.7)	2.0 (2.0)	3.5 (3.3)
CC <sub>1/2</sub>	0.99 (0.96)	0.99 (0.95)	0.99 (0.98)	0.99 (0.73)	0.99 (0.46)	0.99 (0.66)	0.98 (0.60)
<b>Refinement</b>							
Resolution (Å)				1.91	2.55	1.80	2.06
No. reflections				332,570	148,575	454,150	280,985
<i>R</i> <sub>work</sub> / <i>R</i> <sub>free</sub>				0.19/0.22	0.21/0.245	0.21/0.23	0.21/0.24
<b>No. atoms</b>							
Protein				31506	31388	31597	31482
Ligand/ion				175/6*	66/6	148/6	90/6
Water				1902	159	1666	1029
<b>B-factors (Å<sup>2</sup>)</b>							
Protein				33	54	42	49
Ligand/ion				42/27	48/46	35/49	33/35
Water				34	40	43	37
<b>R.m.s. deviations</b>							
Bond lengths (Å)				0.008	0.009	0.008	0.01
Bond angles (°)				1.4	1.5	1.4	1.6

\*ligands in the uncomplexed structure are derived from ethylene glycol, tartrate / chloride

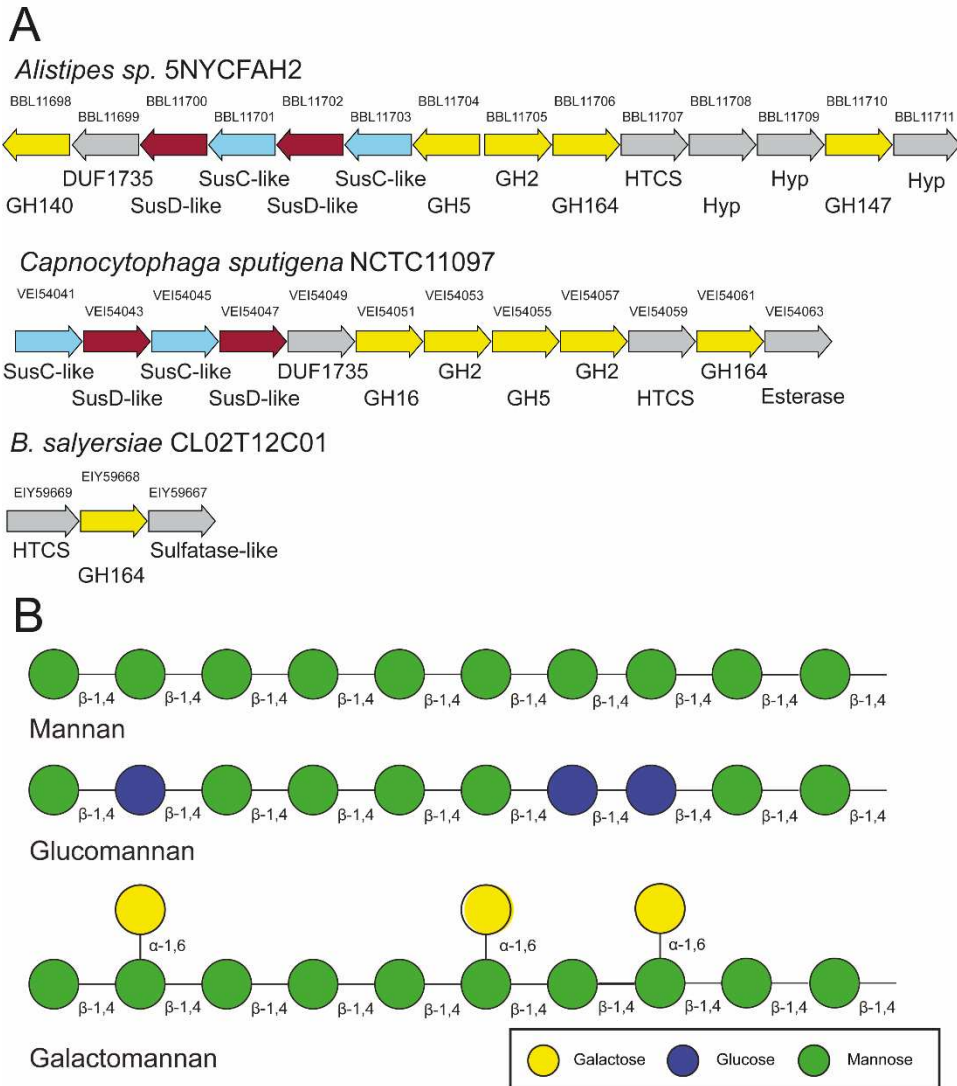


**Figure 1. Genomic context of GH164 enzymes and mannan structure. (A)** Genomic context of the GH164 genes present in the genomes of *B. salyersiae*, *Alistipes* sp. and *C. sputigena*. Locus tags are given above the arrows and predicted annotation is given below. Genes predicted to be GHs are highlighted in yellow, while the SusC-like and SusD-like proteins are shown in blue and burgundy respectively. Genes are not shown to scale. Hybrid two-component systems are abbreviated ‘HCTS’ while hypothetical proteins are annotated ‘Hyp’. None of the GH5 or GH16 genes are currently annotated as belonging to specific subfamilies. **(B)** Mannans and glucomannans contain  $\beta$ -1,4-linked D-mannose residues in their structural backbone with glucomannans also containing backbone  $\beta$ -1,4-linked D-glucose residues. This backbone can be decorated with acetyl groups at the 2- and 3-positions or with  $\alpha$ -linked galactosyl groups at the 6-position, forming galactoglucomannans (41).

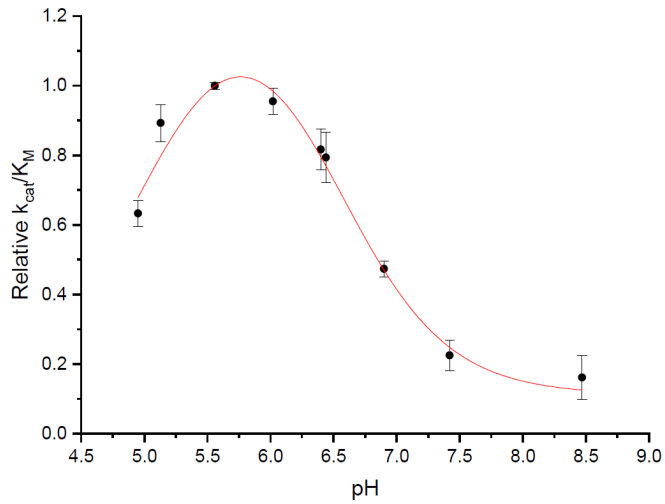


**Figure 2. pH profile of Bs164 activity.** Specificity constants for the hydrolysis of MU  $\beta$ -man were determined between pH 5.0 and 8.5 using substrate depletion kinetics. MES buffer was used between 5.0 and 6.5 and HEPES buffer was used from pH 6.5-8.5.

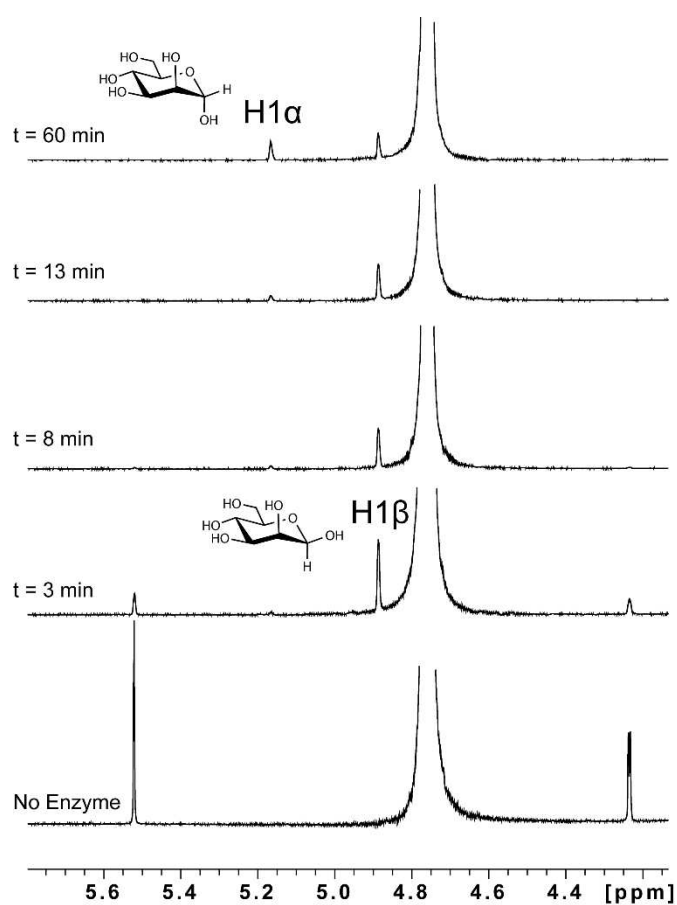


**Figure 3.** *Bs164* acts with retention of stereochemistry. pNP β-man was incubated with *Bs164* and the stereochemistry of the reaction was monitored by <sup>1</sup>H NMR spectroscopy. Before enzyme addition there are no anomeric protons corresponding to free mannose. At  $t = 3$  min, a single new peak corresponding to the H1β of mannose is observed at  $\delta$  4.88 ppm. Mutarotation of the anomer results in a decrease in the H1β signal and an increase of the H1α signal at  $\delta$  5.16 ppm over time.



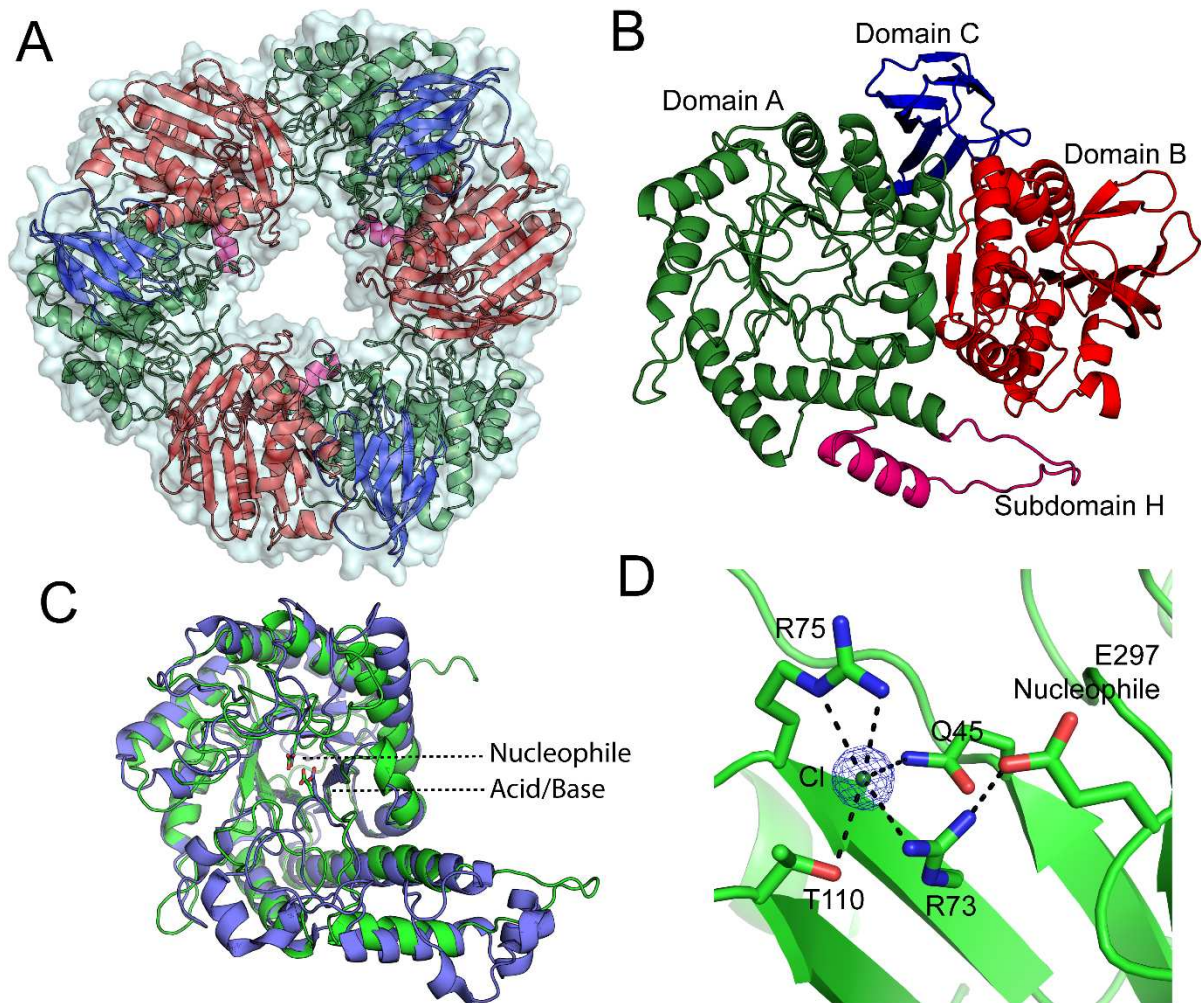


**Figure 4. Structure of Bs164.** The trimeric structure of *Bs164* is shown in panel **A**. All three protomers are shown with a surface and each chain is displayed as a cartoon diagram coloured by domain. **B** shows the structure of one protomer. Domain A, which has a  $(\beta/\alpha)_8$  fold, is shown in green with subdomain H is shown in magenta, domain B, containing a mixed  $\beta$ -sheet, is shown in red and the  $\beta$ -sandwich of domain C is shown in blue. Overlay of domain A of *Bs164* and the catalytic domain of  $\beta$ -galactosidase from *Rahnella sp.* R3 (5E9A) is shown in panel **C**. *Bs164* is in green while 5E9A is coloured blue. Both the catalytic nucleophile and acid/base residue of both structures are shown as sticks. The chlorine binding site of *Bs164* is shown in **D**, with dashed lines showing polar interactions closer than 3.4 Å apart. Electron density for the chloride is a  $\sigma_A$ -weighted  $2F_o - F_c$  density contoured at  $3\sigma$  and rendered with the program PyMol. The nucleophile residue Glu297 is also shown as it interacts with Arg73.

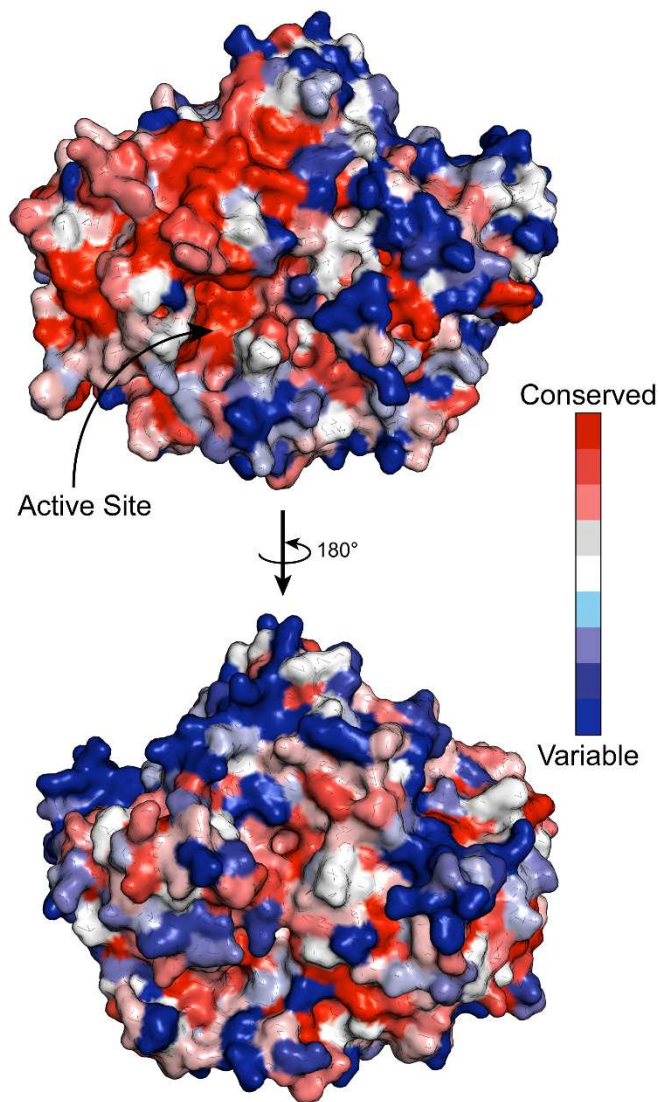


**Figure 5. Conservation of GH164 surface.** Surface representation of *Bs164* colored by sequence conservation within the GH164 family. The figure was prepared using the CONSURF server (40) and generated in PyMol. The top representation is in the same orientation as Figure 3B.

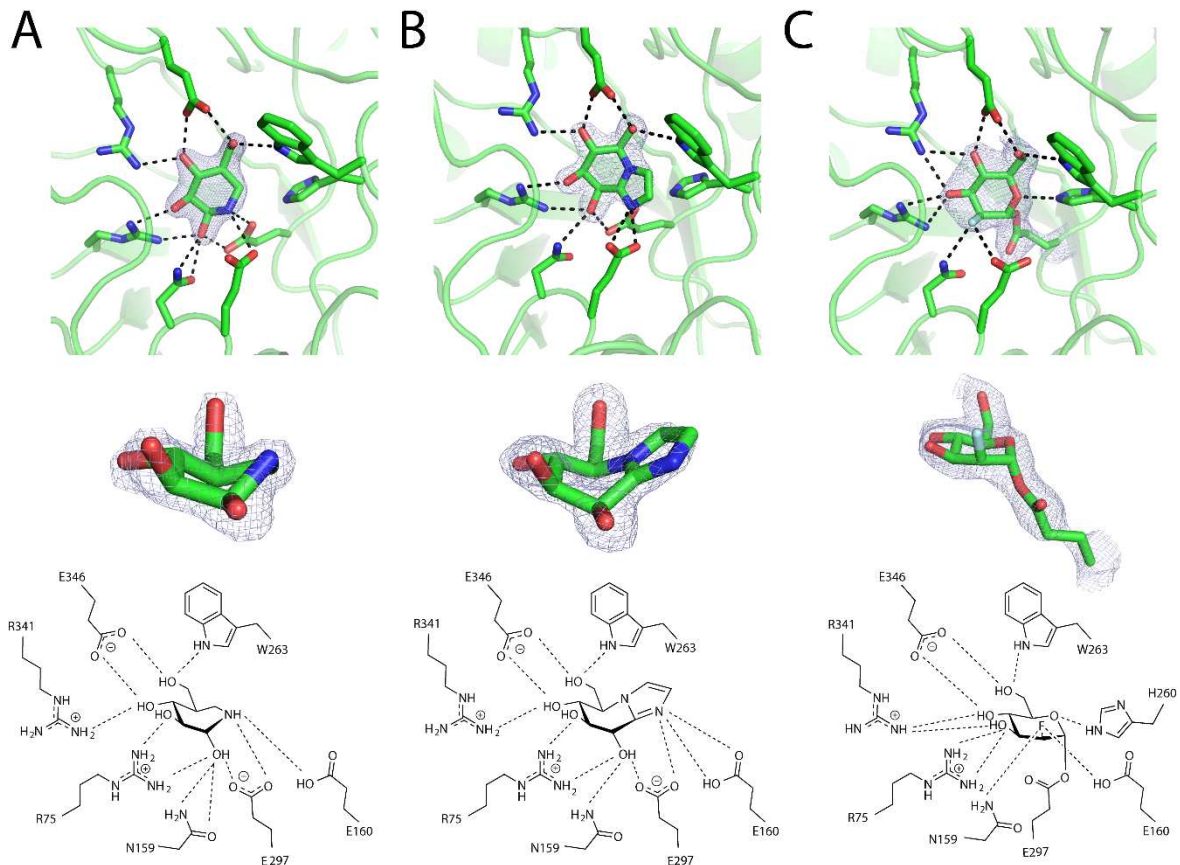


**Figure 6.** Complexes of *Bs164* with inhibitors. (A) Complex with neuromycin (B) complex with mannoimidazole and (C) a complex with covalently bound 2-deoxy-2-fluoro-mannose. The top panel shows the inhibitor within the active site with polar interactions within 3.2 Å shown as black dashed lines. The middle panel shows the inhibitor with the surrounding electron density and the bottom panel shows a cartoon schematic of active site interactions. All electron density meshes are  $\sigma_A$ -weighted  $2F_o - F_c$  densities contoured at  $1.5 \sigma$  and rendered with the program PyMol. Trp336, which sits below the inhibitors, has been omitted for clarity.

**Structure and function of Bs164  $\beta$ -mannosidase from *Bacteroides salyersiae* the founding member of glycoside hydrolase family GH164**

Zachary Armstrong and Gideon J Davies

*J. Biol. Chem.* published online December 22, 2019

---

Access the most updated version of this article at doi: [10.1074/jbc.RA119.011591](https://doi.org/10.1074/jbc.RA119.011591)

Alerts:

- [When this article is cited](#)
- [When a correction for this article is posted](#)

[Click here](#) to choose from all of JBC's e-mail alerts